View metadata, citation and similar papers at core.ac.uk
brought to you by CORE
provided by DSpace@MIT

Spatially Continuous Depletion Algorithm for Monte Carlo Simulations

Matthew S. Ellis,* Colin Josey,† Benoit Forget, Kord Smith

Massachusetts Institute of Technology, 77 Massachusetts Avenue, Cambridge, MA
**mellis13@mit.edu, †cjosey@mit.edu*

INTRODUCTION

To correctly predict reactor behavior during cycle operations, the evolution of nuclide number densities throughout the core must be accurately modeled. The time-varying spatial distribution of nuclide number densities is typically resolved by discretizing the Monte Carlo geometry into smaller cells over which number densities are assumed to be spatially invariant. The nuclide number densities in these smaller cells are integrated through time using reaction rate tallies on the same discretized geometry. However, detailed distributions of nuclide number densities in a full three dimensional simulation can require a prohibitive amount of tallies, and the spatial discretization of the base geometry makes coupling to external multiphysics tools difficult.

In this paper a method for solving for spatially continuous number density distributions during depletion calculations will be described. The spatially continuous number densities can be used in the transport method proposed by Brown and Martin [1] which allows for transporting neutrons through a material with continuously varying properties such as temperature and nuclide number densities. Coupled with the ability of Functional Expansion Tallies (FETs) [2] to represent tallied quantities as continuous functions, it is possible to both solve for and make use of spatially continuous nuclide number densities. The need for this capability was alluded to by Brown et. al. [3], but no solution has yet been proposed. With a continuous depletion method, recent work which utilized FETs and continuous material tracking to incorporate multiphysics feedback in Monte Carlo simulations can be extended to simulations that include depletion analysis [4, 5].

THEORY

The rate of change of a nuclide's number density is described by the balance equation below [6]:

$$\begin{aligned}\frac{dN_i(t,\boldsymbol{r})}{dt} &= \sum_j \left[\int_0^\infty \gamma_{ji}(E,t)\sigma_{f_j}(E,t,\boldsymbol{r})\phi(E,t,\boldsymbol{r})dE\right] N_j(t,\boldsymbol{r}) \\ &+ \left[\int_0^\infty \sigma_{c_{i-1}}(E,t,\boldsymbol{r})\phi(E,t,\boldsymbol{r})dE\right] N_{i-1}(t,\boldsymbol{r}) + \lambda_{i'} N_{i'}(t,\boldsymbol{r}) \\ &- \left[\int_0^\infty \left(\sigma_{f_i}(E,t,\boldsymbol{r}) + \sigma_{c_i}(E,t,\boldsymbol{r})\right)\phi(E,t,\boldsymbol{r})dE\right] N_i(t,\boldsymbol{r}) \\ &- \lambda_i N_i(t,\boldsymbol{r}) \end{aligned} \quad (1)$$

where,

$N(t,\boldsymbol{r})$ ≡ number density of a nuclide
$\gamma_{ji}(E,t)$ ≡ fission production yield of nuclide i from nuclide j
$\phi(E,t,\boldsymbol{r})$ ≡ neutron flux
λ ≡ decay constant of a nuclide
$\sigma_f(E,t,\boldsymbol{r})$ ≡ microscopic fission cross section of a nuclide
$\sigma_c(E,t,\boldsymbol{r})$ ≡ microscopic capture cross section of a nuclide

Note that in the above equations the fission product yield and decay constants are assumed to be spatially invariant. Now, the number densities can be expanded as a weighted sum of a polynomial basis set:

$$N_i(t,\boldsymbol{r}) = \sum_\alpha N_{i,\alpha}(t)P_\alpha(\boldsymbol{r}) \quad (2)$$

where α denotes the indices for the moments in a three dimensional space. The coefficients, N_α, of the number density polynomial expansion are calculated using the following integral expressions:

$$\int_V d\boldsymbol{r}P_\gamma(\boldsymbol{r})N_i(t,\boldsymbol{r}) = \sum_\alpha N_{i,\alpha}(t)\int_V d\boldsymbol{r}P_\alpha(\boldsymbol{r})P_\gamma(\boldsymbol{r}) \quad (3)$$

$$\int_V d\boldsymbol{r}P_\gamma(\boldsymbol{r})N_i(t,\boldsymbol{r}) = \sum_\alpha N_{i,\alpha}(t)C_{\alpha,\gamma} \quad (4)$$

If an orthogonal basis set is chosen, the expression in Eq. (4) simplifies to:

$$\int_V d\boldsymbol{r}P_\gamma(\boldsymbol{r})N_i(t,\boldsymbol{r}) = N_{i,\gamma}(t)C_\gamma \quad (5)$$

The microrates in Eq. (1) can be similarly expanded. Eq. (6) shows the expansion for an arbitrary microrate reaction, x. The coefficients for the microrate expansions, R^x_β, are determined in the Monte Carlo simulation using FETs [2], and the FET polynomials, $P_\beta(\boldsymbol{r})$, are assumed to belong to an orthogonal basis set.

$$\int_0^\infty dE\phi(E,t,\boldsymbol{r})\sigma_x(E,t,\boldsymbol{r}) = \sum_\beta R^x_\beta(t)P_\beta(\boldsymbol{r}) \quad (6)$$

The number density and microrate expansions can be substituted back into Eq. (2). To make this substitution useful, the entire expression is multiplied by one of the number density polynomials, $P_\gamma(\boldsymbol{r})$, and integrated over the volume. From this point on it is assumed that the polynomial basis set used for the number densities is orthogonal. With some algebraic simplification, the following expression is obtained:

$$\begin{aligned} C_\gamma \frac{dN_{i,\gamma}(t)}{dt} &= C_\gamma\lambda_{i'}N_{i',\gamma} - C_\gamma\lambda_i N_{i,\gamma} \\ &\sum_{j,\alpha,\beta} R^{f,j\to i}_\beta(t)N_{j,\alpha}(t)\int_V d\boldsymbol{r}P_\gamma(\boldsymbol{r})P_\beta(\boldsymbol{r})P_\alpha(\boldsymbol{r}) \\ &+ \sum_{\alpha,\beta} R^{c,i-1,i}_\beta(t)N_{i-1,\alpha}(t)\int_V d\boldsymbol{r}P_\gamma(\boldsymbol{r})P_\beta(\boldsymbol{r})P_\alpha(\boldsymbol{r}) \\ &- \sum_{\alpha,\beta}\left(R^{f,i}_\beta(t) + R^{c,i}_\beta(t)\right)N_{i,\alpha}(t)\int_V d\boldsymbol{r}P_\gamma(\boldsymbol{r})P_\beta(\boldsymbol{r})P_\alpha(\boldsymbol{r}) \end{aligned} \quad (7)$$

In Eq. (7) the volume integral of the triple product of the polynomials does not easily simplify. However, these triple product integrals can be computed for the chosen basis sets up to a predetermined order. These precomputed coefficients will be denoted by $B_{\alpha,\beta,\gamma}$. This simplification yields the final expression:

$$\begin{aligned} C_\gamma \frac{dN_{i,\gamma}(t)}{dt} &= C_\gamma \lambda_{i'} N_{i',\gamma} - C_\gamma \lambda_i N_{i,\gamma} \\ &+ \sum_{j,\alpha,\beta} R_\beta^{f,j\to i}(t) N_{j,\alpha}(t) B_{\alpha,\beta,\gamma} \\ &+ \sum_{\alpha,\beta} R_\beta^{c,i-1,i}(t) N_{i-1,\alpha}(t) B_{\alpha,\beta,\gamma} \\ &- \sum_{\alpha,\beta} \left(R_\beta^{f,i}(t) + R_\beta^{c,i}(t) \right) N_{i,\alpha}(t) B_{\alpha,\beta,\gamma} \end{aligned} \tag{8}$$

When solving for the spatial distribution of number densities as a function of time, Eq. (8) will yield a system of ordinary differential equations with the number of unknowns equal to the total sum of the number of expansion coefficients for all nuclides. Note that this derivation allows for each nuclide to have a different expansion order for number density. The system of ODEs is of the form:

$$\frac{d\boldsymbol{N}_{\boldsymbol{\gamma}}(t)}{dt} = \boldsymbol{A}(t)\boldsymbol{N}_{\boldsymbol{\gamma}}(t) \tag{9}$$

For constant coefficients, the solution of the system of ODEs is the following matrix exponential expression:

$$\boldsymbol{N}_{\boldsymbol{\gamma}}(t) = e^{\boldsymbol{A}t}\boldsymbol{N}_{\boldsymbol{\gamma}}(t_0) \tag{10}$$

Eq. 9 and Eq. 10 are of the same form as traditional depletion systems. However, in the case of spatially continuous depletion, the unknowns in the vector are coefficients for each moment in the expansion instead of cell average number densities.

RESULTS AND ANALYSIS

The spatially continuous depletion method was tested using the open source Monte Carlo code OpenMC [7]. FETs were implemented in OpenMC using the Zernike polynomials [8] as a basis set and the 48-term CRAM solver proposed by Pusa [9] was used to evaluate the matrix exponential for one time step. In this paper, when the order of expansion for the nuclide number densities is specified, it is assumed that the microrate tallies are of the same order. The depletion calculations were performed using external Python scripts that utilize the OpenMC Python API.

The continuous depletion methodology was tested on a simple problem shown in Figure 1. The test problem consists of nine fuel pellets with accompanying gas gap and cladding, and the domain is surround by reflective boundary conditions. The center fuel pin contains 2% (weight) Gd-157 and will be the pin that is depleted for comparison purposes.

The center pin contains U-235, U-238, Gd-157, and O-16 at the beginning of life, and I-135, Xe-135, Xe-136, Cs-135, Gd-156, Gd-157, U-234, U-235, and U-238 were included in the depletion matrix. The depletion step that will be shown in the following results spans from $t = 0$ to $t = 2$ months. The simulation ran 1 million particles per batch with 60 active batches and 40 inactive batches. The reference case which will be used to assess the continuous depletion results is an equal volume discretization of the central pellet into 50 equal volume rings with 32 azimuthal cuts. It is worth noting that for the number of particles simulated the depletion matrix satisfied the negative eigenvalue criterion for CRAM. However, for an extremely low number of neutrons per batch (i.e. 100), positive eigenvalues were observed.

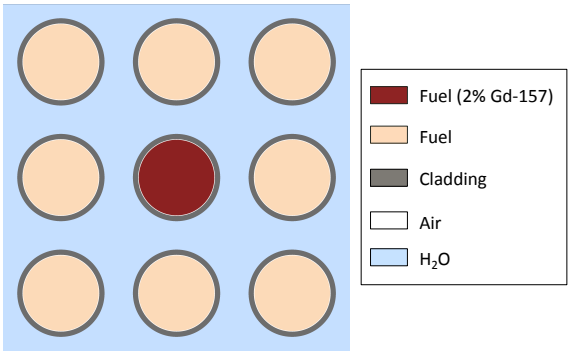

Fig. 1. OpenMC geometry model colored by unique material composition

Depletion Results

Figure 2 shows the calculated number density for Xe-135 for Zernike expansions of order 2, 6, and 10. The continuous depletion results were integrated into the same volumes that characterize the discrete case so that a direct comparison of errors between the two solution methods is possible. Note that the abscissa is a cell index instead of a coordinate position. Cell indices are ordered from the origin with sweeps through azimuthal cuts followed by radial rings.

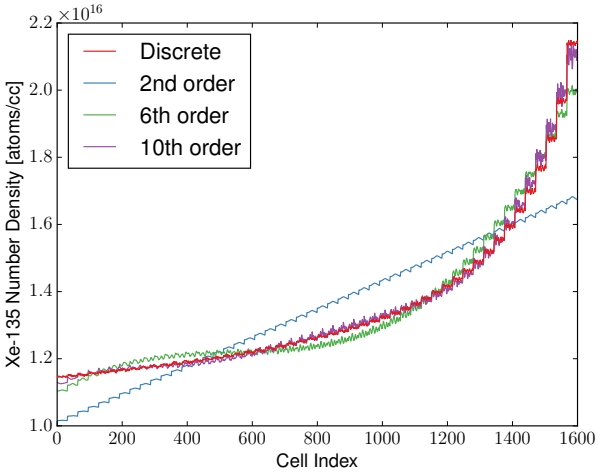

Fig. 2. Xe-135 number density for Zernike expansion of order 2, 6 and 10, compared to a pin discretized with 50 equal volume rings with 32 azimuthal cuts

Figure 2 shows that there is very little azimuthal variation in the number densities for this simulation, and that for a 10th order expansion the continuous depletion results agree very closely with the discrete case for Xe-135. This is verified quantitatively in Figure 3 where the L2 error between the continuous depletion and discrete depletion methods is shown for the Xe-135 solution.

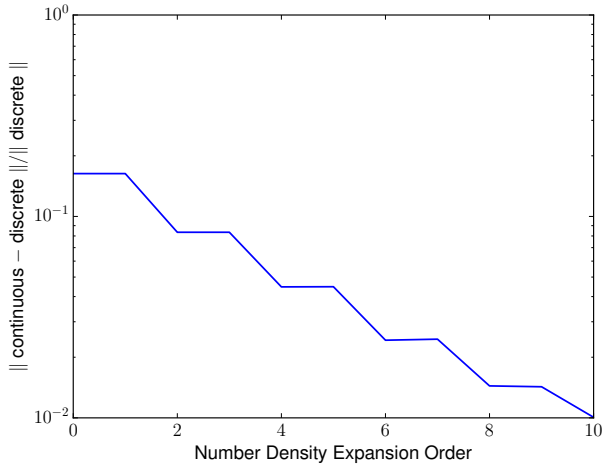

Fig. 3. L2 error of the Xe-135 continuous number density solution as compared to the discrete reference solution

Figure 4 and Figure 5 show the calculated number density for Gd-157 for 2, 6, and 10th order Zernike expansions with linear and logarithmic scales, respectively. Unlike the Xe-135 number density profile, the Gd-157 spatial distribution is much harder to capture with the Zernike polynomial basis set. This limitation is evident by the negative number densities obtained at the periphery of the pin.

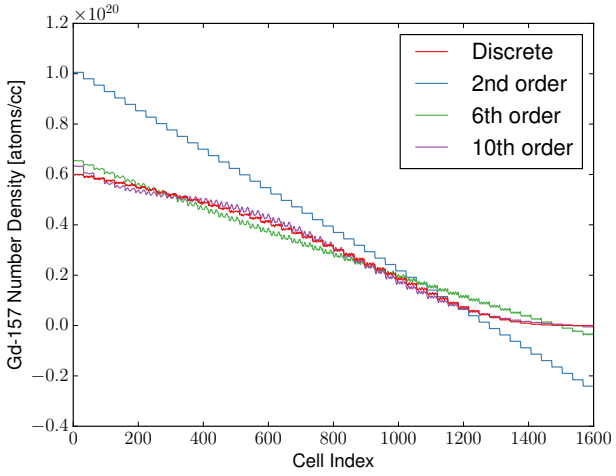

Fig. 4. Gd-157 number density (linear scale) for Zernike expansion of order 2, 6 and 10, compared to a pin discretized with 50 equal volume rings with 32 azimuthal cuts

The Gd-157 radial number density distribution is one of the most challenging distributions to represent with a polynomial expansion because of the nearly five order of magnitude variation from the center of the pin to a position offset from the pellet surface that shifts inward as the pin is depleted. Figure 4 and Figure 5 show that as the number density expansion order is increased, the prediction of negative number densities is confined to fewer radial rings. However, even with a higher

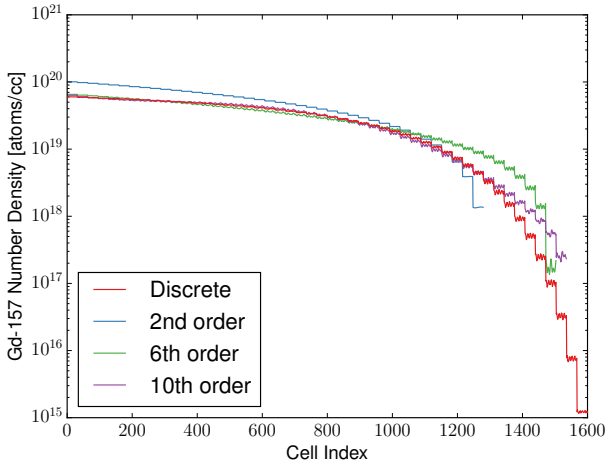

Fig. 5. Gd-157 number density (logarithmic scale) for Zernike expansion of order 2, 6 and 10, compared to a pin discretized with 50 equal volume rings with 32 azimuthal cuts

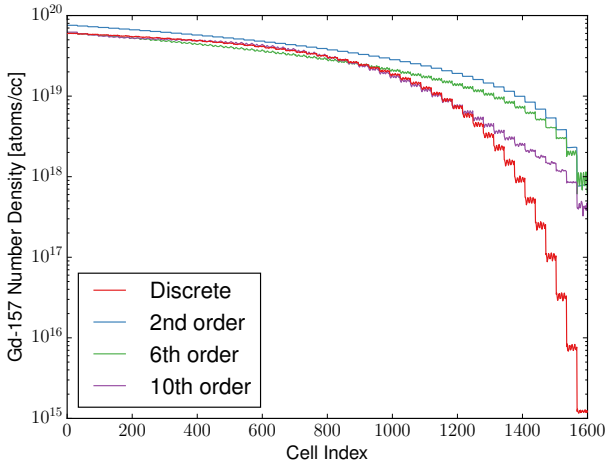

Fig. 6. Gd-157 number density for Zernike expansion of order 2, 6 and 10, with scaled coefficients to eliminate negative Gd-157 number density predictions

order expansion, it is impossible to guarantee that the number density will be positive everywhere. As a result, a post processing correction has been implemented to scale all non-zeroth order expansion coefficients of the nuclide number density by a single factor to guarantee that all number densities in the domain remain positive. It is important to note that by only scaling the non-zeroth order expansion coefficient, the total mean nuclide densities are not altered. The Gd-157 number density results after scaling the coefficients is shown in Figure 6. Note that the scaling has minor effects in the interior of

the pin where the number density is much larger than on the periphery of the pin. The L2 error for the scaled and unscaled Gd-157 number density solutions are shown in Figure 7.

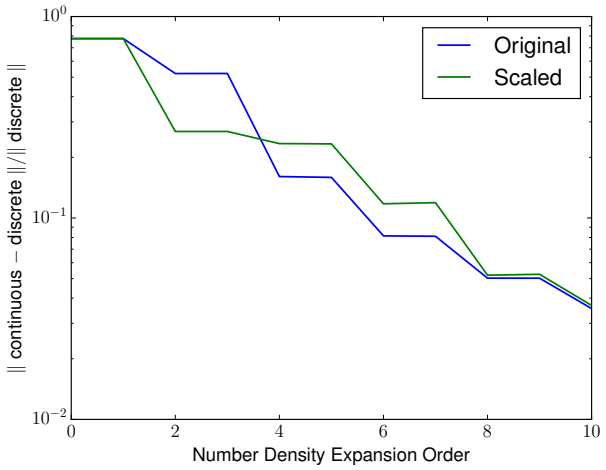

Fig. 7. L2 error of the Gd-157 continuous number density solution with scaled and unscaled coefficients as compared to the discrete reference solution

CONCLUSIONS

A methodology for calculating spatially continuous distributions of number densities in a burnup calculation was successfully demonstrated in this paper. It was shown that for a single depletion step of two months the continuous depletion methodology using Zernike basis functions was capable of accurately predicting the spatial distribution of Xe-135 in an LWR fuel pin. However, for nuclides such as Gd-157 with distributions not easily represented by the Zernike functions, the prediction of nuclide number densities showed inaccuracies. More specifically, the predictions included negative number densities for the Gd-157 spatial distribution. It was shown that a post processing step to scale all expansion coefficients except for the zeroth moment could remove the negative number densities without having a large effect on the overall error of the solution. However, this post processing methodology requires additional analysis before being put forth as the ideal solution.

FUTURE WORK

The test problem used to demonstrate the continuous depletion methodology was limited to five nuclides at the beginning of life, and only nine nuclides were followed through the single depletion step. While the depletion behavior of Gd-157 provides a good test for the methodology, a larger set of isotopes should be examined to determine the appropriateness of this method for full reactor analyses. Additionally, the microrates that were tallied using FETs need to examined to determine the appropriateness of the Zernike basis set and the effect of microrate uncertainty and truncation error on the continuous depletion solution in LWR applications. The most important next step is the use of the continuous depletion solution in the Monte Carlo calculation in order to perform multistep depletion calculations. This will not only test the continuous tracking methodology with multiple varying nuclides, but also extend the multiphysics coupling capabilities that initially inspired this paper.

ACKNOWLEDGMENTS

This material is based upon work supported by the Idaho National Laboratory under DOE Idaho Operations Office Contract DE-AC07-05ID14517 and by the Department of Energy Nuclear Energy University Programs Graduate Fellowship.

REFERENCES

1. F. B. BROWN and W. R. MARTIN, "Direct sampling of Monte Carlo flight paths in media with continuously varying cross-sections," in "Proc. ANS Mathematics & Computation Topical Meeting," (2003), vol. 2.
2. D. P. GRIESHEIMER, W. R. MARTIN, and J. P. HOLLOWAY, "Convergence properties of Monte Carlo functional expansion tallies," *Journal of Computational Physics*, **211**, *1*, 129 – 153 (2006).
3. F. B. BROWN, D. GRIESHEIMER, and W. R. MARTIN, "Continuously varying material properties and tallies for Monte Carlo calculations," *Proceedings of the Physics of Fuel Cycles and Advanced Nuclear Systems: Global Developments, Chicago, Illinois, April*, pp. 25–29 (2004).
4. M. ELLIS, D. GASTON, B. FORGET, and K. SMITH, "Preliminary Coupling of the Monte Carlo Code OpenMC and the Multiphysics Object-Oriented Simulation Environment (MOOSE) for Analyzing Doppler Feedback in Monte Carlo Simulations," *ANS MC2015 - Joint International Conference on Mathematics and Computation (M&C), Supercomputing in Nuclear Applications (SNA) and the Monte Carlo (MC) Method* (April 2015).
5. M. ELLIS, D. GASTON, B. FORGET, and K. SMITH, "Continuous Temperature Representation in Coupled OpenMC/MOOSE Simulations," *PHYSOR 2016 - Unifying Theory and Experiments in the 21st Century* (May 2016).
6. P. J. TURINSKY, *Handbook of Nuclear Engineering*, Springer US, Boston, MA, chap. Core Isotopic Depletion and Fuel Management, pp. 1241–1312 (2010).
7. P. K. ROMANO and B. FORGET, "The OpenMC Monte Carlo particle transport code," *Annals of Nuclear Energy*, **51**, 274–281 (2013).
8. VON F. ZERNIKE, "Beugungstheorie des schneidenverfahrens und seiner verbesserten form, der phasenkontrastmethode," *Physica*, **1**, *7*, 689 – 704 (1934).
9. M. PUSA, "Higher-Order Chebyshev Rational Approximation Method and Application to Burnup Equations," *Nuclear Science and Engineering*, **182**, *3*, 297–318 (2016).